PROCEEDINGS, 48th Workshop on Geothermal Reservoir Engineering
Stanford University, Stanford, California, February 6-8, 2023
SGP-TR-224

Development Update on Chloride-based Inflow Measurement in Fractured Enhanced Geothermal Systems (EGS) Wells

Luthfan Hafizha Judawisastra[1], Sarah Sausan[1], Jiann-cherng Su[2] and Roland N. Horne[1]

[1]Dept. of Energy Science and Engineering, Stanford University

[2]Sandia National Laboratories

luthfan@stanford.edu, sausan@stanford.edu, jsu@sandia.gov, horne@stanford.edu

Keywords: chloride concentration, feed zone, fracture inflows, single phase, EGS, Utah FORGE

ABSTRACT

This paper discusses the ongoing development of a chloride-based inflow measurement tool for detecting and quantifying inflows in enhanced geothermal system (EGS) wells. Initial field testing will commence at Utah FORGE (Frontier Observatory for Research in Geothermal Energy), with the goal of implementation to other EGS sites. Specifically, this paper describes the current progress and results of laboratory experiments, numerical flow simulation, and the assembly of a new prototype of the tool by Sandia National Laboratory. The new version of the tool is being built to withstand high pressure and high temperature conditions and will be tested at 207 MPa and 225°C. Laboratory experiments confirm that measurements directly in front of the feed zone results in significantly higher accuracy in chloride concentration estimation. Furthermore, additional dye-tracer cross sectional view laboratory experiments show similar flow behaviors to those observed in the numerical simulation results. The simulation results agreed with the experimental measurements, particularly in observing the peak chloride concentration at the feed zone height. However, some differences were found in the measured concentration, suggesting that the calibration equation needs to be adjusted. The simulation also showed that measurement zones are more significant in high inlet flow rate cases than in low inlet flow rate cases, but the inlet front peak can still be detected. Furthermore, the simulation of various tool position scenarios indicates that inlet front peak chloride concentrations are only registered to high precision within the feed zone "jet" and may need correction if measured outside the jet. Overall, the findings support the inclusion of a centralizer for the wireline tool design to increase the consistency and precision of the chloride concentration calculation. The successful development and deployment of this tool will reduce uncertainty in EGS well development and make EGS more commercially viable.

1. INTRODUCTION

An Enhanced Geothermal System (EGS) is harnesses geothermal energy by creating artificial fractures in low-permeability rocks through a process of stimulation (Huenges, 2016). These fractures are created to increase the amount of heat that can be extracted from the subsurface. After these fractures are created, it is important to continuously monitor their effectiveness throughout the life of the well as additional stimulation may be needed to maintain the desired level of productivity. The pressure-temperature spinner (PTS) tool is a commonly used method for measuring the inflow rate from feed zones in EGS wells. However, it has been found that the PTS tool can be unreliable in wells with low fluid velocity, low enthalpy, and large diameters (Acuña and Arcedera, 2005). This project aims to provide an alternative and more reliable method for measuring the inflow rate from feed zones in EGS wells.

This research builds upon and expands a previous study by Gao et al. (2017) to apply to EGS wells, specifically for the conditions and configurations found at Utah FORGE where field tests will be conducted. In the previous study, feed zone enthalpy was measured by proxy of voltage measurement taken using the ion-selective electrode. Chloride was selected as the measurement target considering chloride always remains in the liquid phase which implies a change in chloride concentration reflects a change in steam fraction. In this study, the focus is on measuring the feed zone inflow rate instead of enthalpy, as the approach would be applied for single-phase flow with the primary objective of identifying and quantifying feed zones in EGS wells.

Four methods were used to determine optimal tool design and measuring techniques: analytical derivations, laboratory experiments, numerical flow simulations, and field tests. The initial stage of this ongoing research has been described in Sausan et al. (2022), which included the analytical approach of flow rate estimation based on chloride concentration and field test preliminary data analysis which indicated well 58-32 as the most suitable candidate for the field test at Utah FORGE.

The early prototype of the chloride measurement device was developed at Sandia National Laboratory (Cieslewski et al. 2016; Corbin et al. 2017). The device was designed as a wireline tool that infers chloride concentration via voltage measurement using an ion-selective electrode. Using an empirical relationship, the measured voltage is converted into chloride concentration, which can then be used to estimate the feed zone flow rate via a series of mass balance equations detailed by Sausan et al. (2022).

Early laboratory experiments and numerical simulation progress were outlined in Judawisastra et al. (2022). The laboratory experiments were conducted utilizing the same prototype tool used by Gao et al. (2017). Updated calibration experiments resulted an empirical relationship between voltage and chloride concentration to be:

$$-log(M) = 98.58V + 0.2998 \quad (1)$$

where M and V are chloride concentration in mol/L and voltage in volts, respectively.

It was postulated that the relationship changed due to the device and electrode aging over the five years since the last calibration was performed, thus warranting a new version of the tool to be fabricated.

To simulate field conditions, experiments using the chloride tool were designed with varying wellbore and feed zone configurations using the artificial well system at Stanford Geothermal Laboratory. The first experiments were conducted by flowing the main wellbore without injection ports. Varying chloride concentrations flowed through the wellbore, and measurement was recorded by placing the chloride tool in the reservoir tank and inside the wellbore during circulation. The result was satisfactory up to 0.4 mol/L, as the chloride concentration calculated using the voltage-chloride relationship (Equation 1) was consistent to the known chloride concentration.

The following experiments focused on simulating the inflow from a feed zone by activating one of the injection ports. The downhole flow had no chloride concentration, while chloride solution was injected through the injection port. Three different chloride concentrations of 0.1, 0.5 and 1 mol/L were evaluated. The chloride tool was positioned at the center of the wellbore with the electrode end placed close to the feed zone port. The result shows that it took 2.5 minutes for the voltage measurement to stabilize, which was a considerable amount of time for a wireline operation. It was also observed that the final measurement still underestimated the actual chloride concentration (Figure 1), with higher accuracy for higher chloride concentration. The underestimation was believed to be due to nonuniform mixing and suboptimal placement.

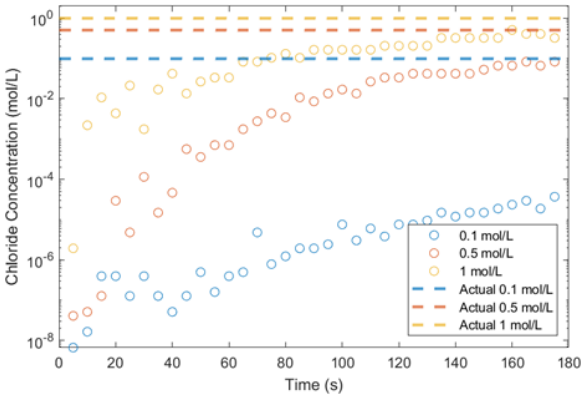

Figure 1: One feed zone calculated chloride concentration result, regenerated from Judawisastra et al. (2022).

The dye tracer test was performed to gain better understanding of the flow dynamics and fluid mixing behavior within the well. Instead of injecting chloride solution as in the previous experiments, blue-dyed fresh water was injected at a rate of 100 ml/s. Results from the test, shown in Figure 2, showed that the inflow fluid initially flowed across the wellbore, hit the opposite wall, and then moved upward following the direction of wellbore circulation. Blind spots appeared showing a region at which measurement would underestimate the injected chloride concentration. Furthermore, the presence of turbulence was indicated by erratic up-and-down movement and alternating fluid paths from curved to straight.

In addition to the laboratory experiments, numerical simulation as described in Judawisastra et al. (2022) examined various simulation cases for Model S1 with a singular jetting point. Case group S1-L4 was set up similarly to the laboratory experiment conditions with internal flow of 2.09 kg/s and wellhead valve open. Various feed zone inflow rates between 5 ml/s to 200 ml/s were simulated. The results showed that inflow started to be able to enter the wellbore at flow rate 20 ml/s and was prominently visible starting at 50 ml/s rate.

From comparison to the laboratory experiments, it was found that the 200 ml/s inflow rate case in S1-L4 case groups were the most similar (Figure 2). The numerical simulation successfully replicated the key features observed in the experiments, such as feed zone inflow hitting the opposite of the wall followed by downward dispersion, formation of blind spots, and periodic turbulence. However, the dye tracer experiment was conducted at around 110 ml/s feed zone inflow rate, which suggests that the simulation results were still underestimating the flow behavior.

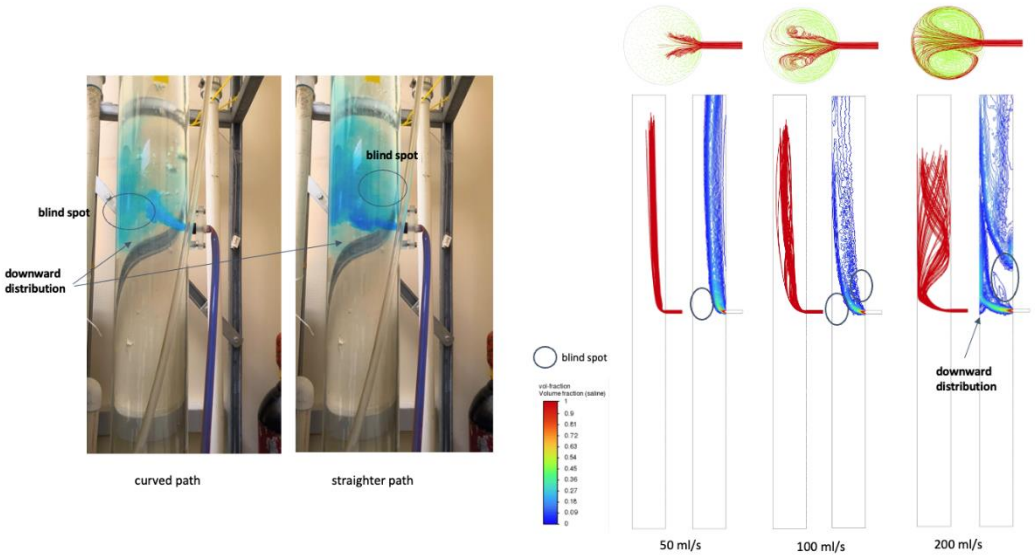

Figure 2: Comparison between lab dye tracer experiment and simulation results of S1-L cases, shown as pathlines and volume fraction graphics X-Z cross-section along with pathlines X-Y cross-section at the inlet location (Judawisastra et al, 2022).

2. UPDATED VERSION TOOL DEVELOPMENT AND ASSEMBLY

The development of an updated version of the chloride tool is currently underway to enhance voltage-chloride calibration and assess its robustness against downhole pressure and temperature conditions that are expected at the Utah FORGE site. Similar to the previous prototype, the new tool version consists of two sensor elements: the chloride ion selective probe and a reference probe. The ion-selective probe generates a voltage that is proportional to the chloride concentration in the fluid while the reference electrode provides the reference potential for pair.

The chloride tool is composed of sensors that are fabricated from powdered feedstocks, which are pressed in die presses. The reference electrode, as shown in Figure 3, comprises of a transducer, a baffle, and a membrane. The transducer is made from silver-coated graphite spheres that are pressed onto the baffle. The baffle is composed of a mixture of silver chloride and potassium chloride powder. The membrane is made from a mixture of potassium chloride and bonding agents, which is pressed in a pellet press and heated to bond to the baffle. A conductor rod that is bonded to the transducer is connected to the exterior of the sealed portion of the autoclave to extract the reference signal.

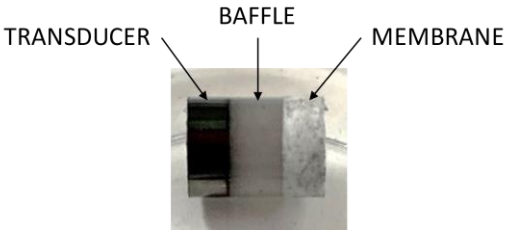

Figure 3: Reference electrode features.

The ion-selective electrode, as shown in Figure 4, is constructed in a similar manner to the reference electrode. However, the sensor pellet is composed of a combination of silver sulfide and silver chloride powders. The sensor is sealed in the autoclave using a PTFE liner and a compression-style tube fitting.

Figure 4: Ion-selective electrode configured for autoclave testing.

The autoclave test conditions, as listed in Table 1, are chosen to replicate the expected conditions for the deployed tool. The autoclave, as shown in Figure 4, allows for the testing of the sensors in a simulated high-pressure, high-temperature environment before the fabrication of the deployable tool. The mechanical integrity and high-temperature calibration of the sensors will be determined during the autoclave tests. The chloride concentration will be adjusted by injecting a brine solution into the autoclave under pressurized conditions.

Table 1: Target conditions for autoclave testing

Pressure	20.7 MPa (3000 psi)
Temperature	225°C (437°F)
Chloride concentration	0.005 mol/L - 0.5 mol/L

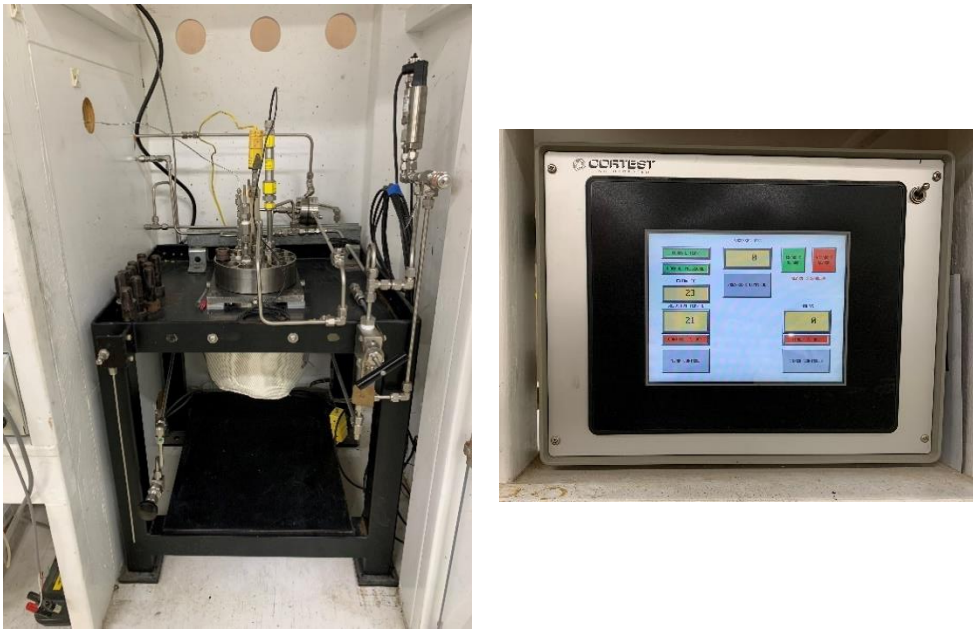

Autoclave Autoclave controller

Figure 5: Sandia Autoclave and Controller.

3. LABORATORY EXPERIMENTS UPDATE

The laboratory experiments were conducted to further evaluate the tool's measurement capability and limitation under various parameters including tool positions, flow rates, and chloride concentrations. Additionally, the experiments also aimed to observe various fluid flow behaviors from the feed zones, which would verify the numerical simulation and provide insights into designing the appropriate operational procedure for the field test.

3.1 Static Measurement

Building on the previous chloride concentration sensitivity experiment conducted by Judawisastra et al. (2022), another static measurement was performed. This measurement involved variations in tool placement, specifically at the center of the wellbore (Position 1) and directly in front of the feed zone (Position 2), as shown in Figure 6. Chloride concentration of 0.1 mol/L was used for the feed zone injection solution considering the result of the previous study which indicates that lower concentration correlates with lower accuracy. The injected solution had an average flow rate of 100 ml/s while the downhole flow rate of the main wellbore circulation system was measured at 2.09 kg/s.

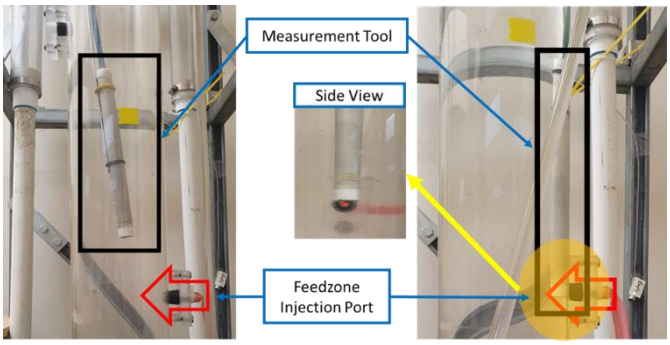

(a) **(b)**

Figure 6: Static measurement assembly (a) Position 1 and (b) Position 2.

The results of voltage measurements are presented in Figure 7a, which shows that at Position 1, measurement drops slowly over time while measurements at Position 2 drop rapidly. Chloride concentration was calculated by using Equation 1, as shown in Figure 7b. It was observed that Position 2 yielded significantly higher accuracy in determining chloride concentration. However, it could be challenging to achieve Position 2 in actual field deployment. Therefore, it is important to understand the range of distance from the feed zone mouth at which the measurement is still acceptably accurate.

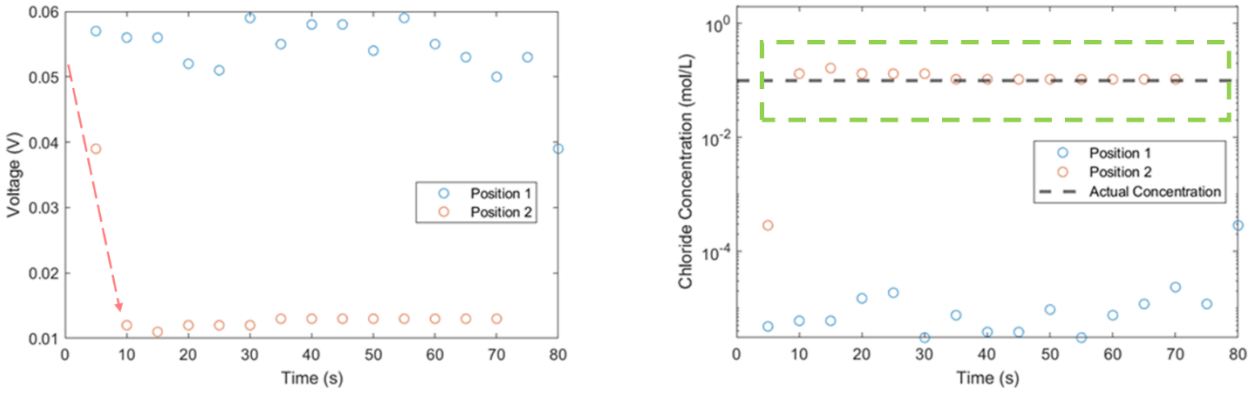

(a) **(b)**

Figure 7: Different tool placement experiments: (a) voltage measurement result, and (b) comparison between calculated and actual chloride concentration values.

3.2 Dye-tracer Test

In addition to the side view observation of the dye-tracer test, a cross-sectional perspective was also achieved by lowering an underwater camera into the flow. Figure 8 shows the cross-sectional view of the blue injection fluid mixed into the wellbore with a 0.5-second increment. The left column shows the actual footage, the middle column shows brightness- and contrast-adjusted footage, and the right column shows the distribution of the blue dye in black. The small red rectangle represents the point where the fluid is being injected, and the circle represents the circumference of the well at that depth. The white rings in the left and middle columns are bubbles on the camera lens, which affects the clarity of the view. However, the original footage still captures the mixing of the dye in the wellbore. From the cross-sectional view captured at taken at 1 second after the injection started (Figure 8c) it can be seen that the injection fluid reached the opposite side of the injection port and swirling to the sides which confirms the observation of the side view. As time goes on, the circling of dye around the perimeter becomes more extensive, resulting a much higher dye distribution around the wellbore seen at Figure 8f.

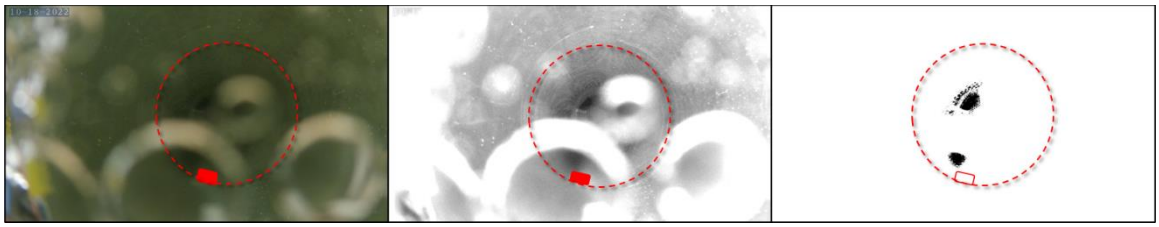

(a)

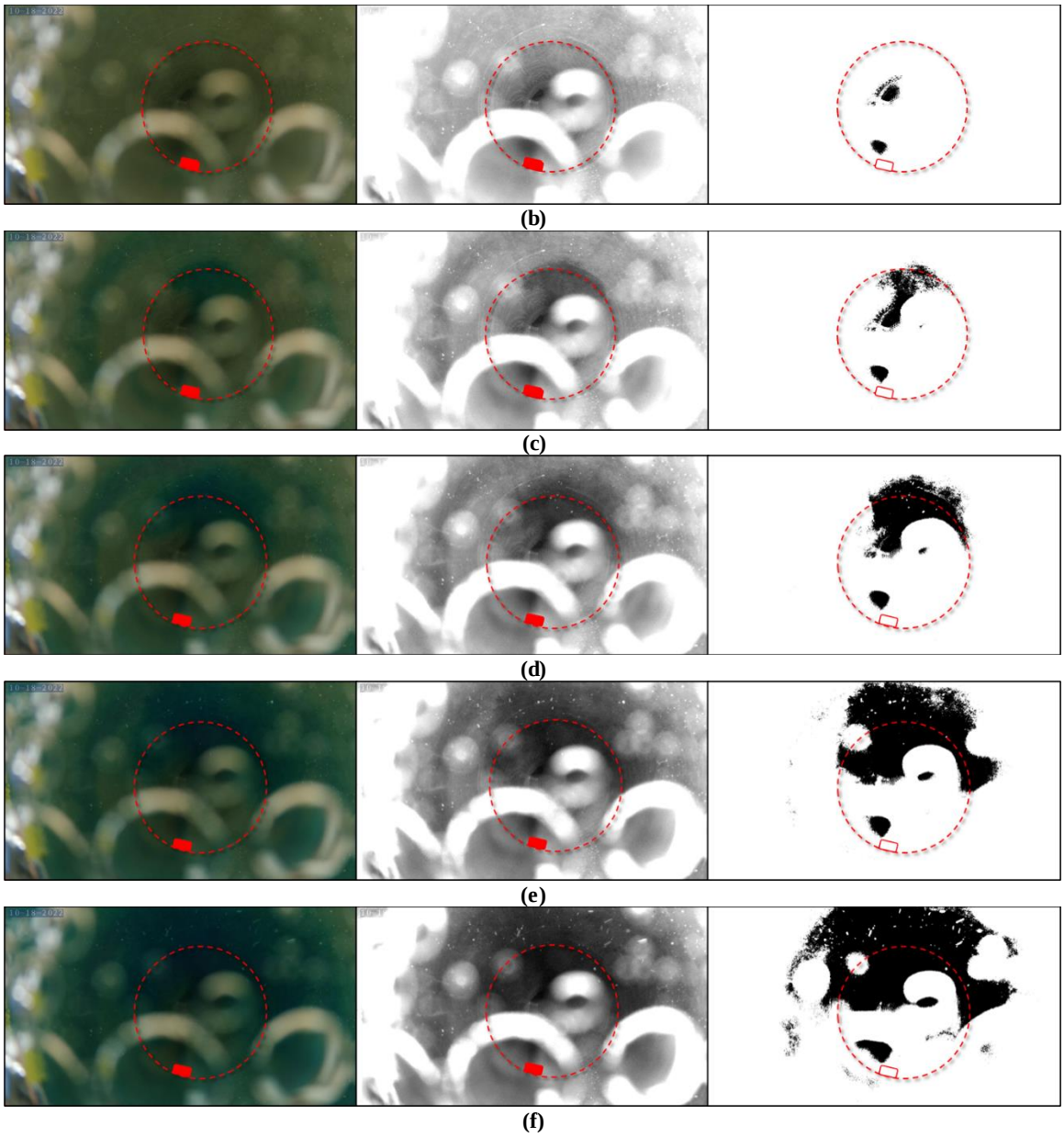

Figure 8: Dye tracer test cross sectional view over time (a) 0 second, (b) 0.5 seconds, (c) 1 seconds, (d) 1.5 seconds, (e) 2 seconds, (f) 2.5 seconds.

To gain a better understanding of the flow behavior, dye tracer tests were conducted under different flow rates of 20, 50, and 70 ml/s, with similar conditions of downhole flow. As the flow became stabilized, a blind spot was observed directly above the feed zone port in the 70 ml/s test (

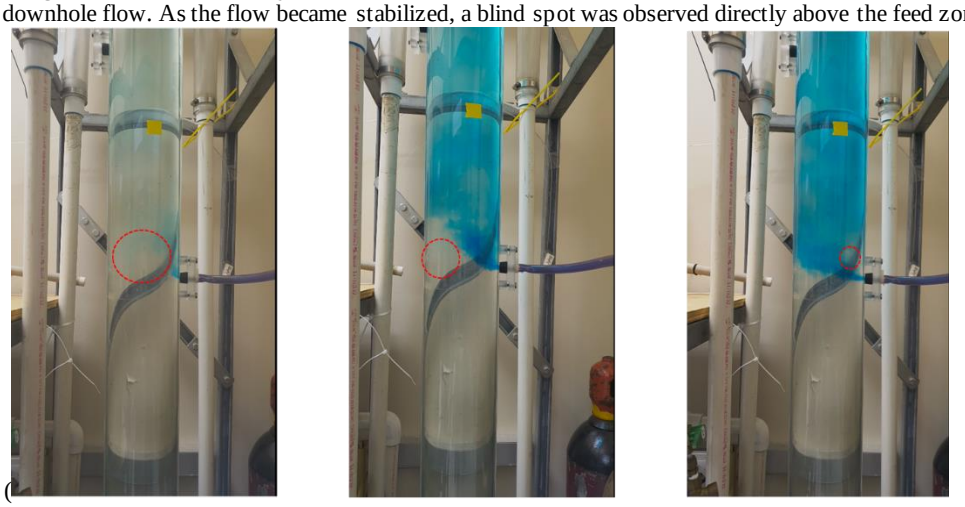

(a) **(b)** **(c)**

Figure 9c), indicated by the red circle. However, this blind spot did not appear in the 20 and 50 ml/s cases. During the 20 ml/s test (

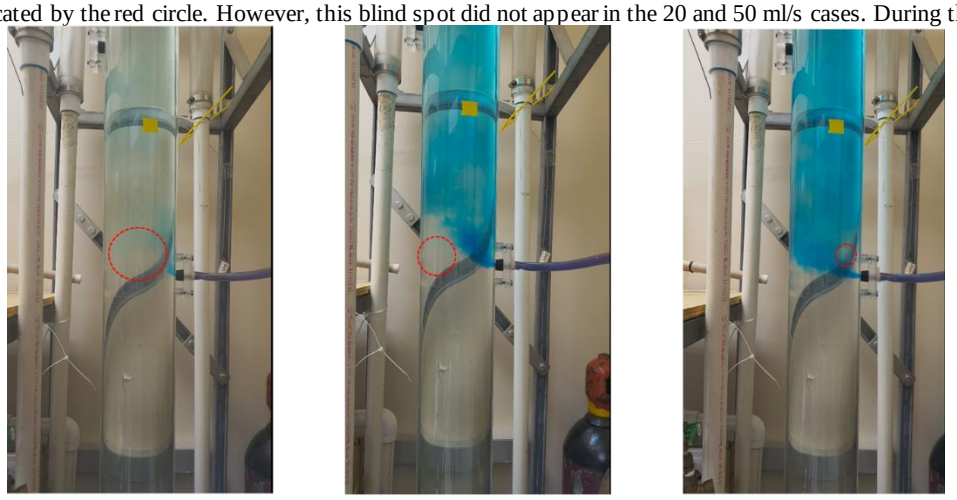

(a) **(b)** **(c)**

Figure 9a), the injection fluid tended to stay on the side wall of the injection port and had less mixing with the downhole flow, while during the 50 ml/s test (

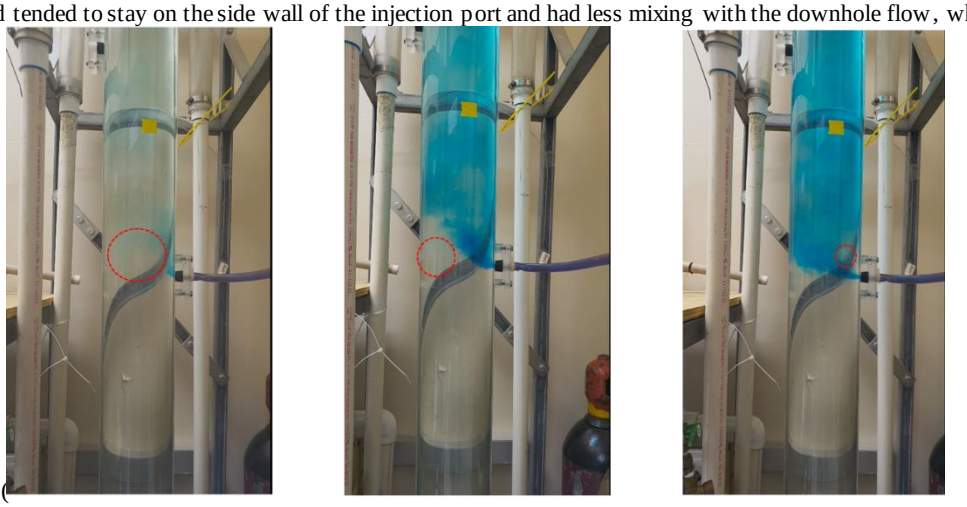

(a) **(b)** **(c)**

Figure 9b), went upward around a third of the well diameter leaving an area without mixing at the other end of the well diameter. The result of these experiments suggest that a higher flow rate produces a blind spot directly above the feed zone inlet, while a lower flow rate produces a blind spot across from the injection port. These findings are consistent with the appearance of blind spots in numerical simulations conducted at low to high feed zone inflow rates, as reported in Judawisastra et al. (2022).

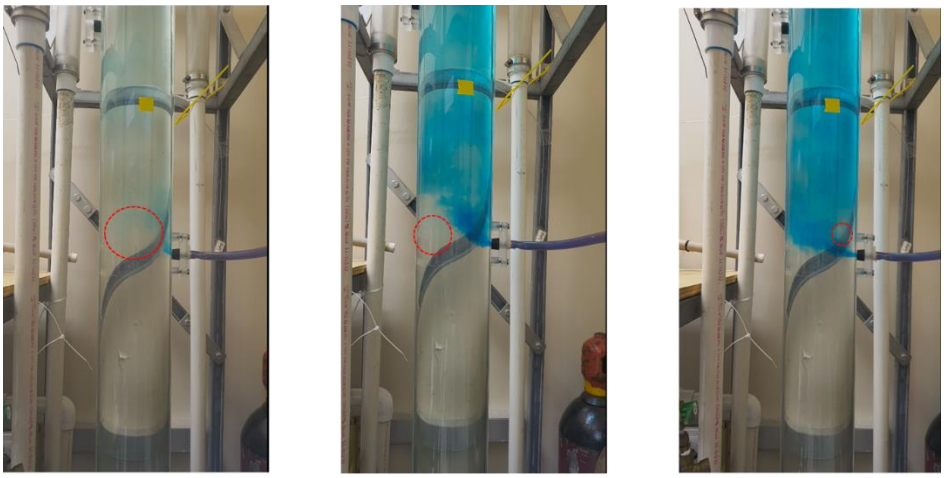

(a) **(b)** **(c)**

Figure 9: Dye injection tracer test (a) 20 ml/s, (b) 50 ml/s, (c) 70 ml/s

3.3 Dynamic Measurement

The dynamic measurement experiments were conducted to replicate the actual field deployment where chloride measurements will be taken along the wellbore using a downhole logging tool attached to a wireline that is in motion during logging. The measurements were conducted by running the tool into the artificial wellbore system, starting from the top to the bottom of the well (run-in hole or RIH) and then pulling the tool back up (pull-out of hole or POOH). The tool was lowered and pulled at a speed of 150 cm/minute. Two measurements were performed under different tool positions. The first measurement was conducted with the tool close to the opposite wall of the injection port (Figure 10a). and the second measurement was run with the tool placed at the center of the wellbore, aided by a centralizer (Figure 10b). The fluid concentration from the injection port was 0.05 mol/L with a flow rate of around 100 ml/s, while the main wellbore flow had a zero chloride concentration with 2.09 kg/s mass rate. Due to limitations of the artificial well system, the measurements were only conducted until a portion of the wellbore section was below the feed zone.

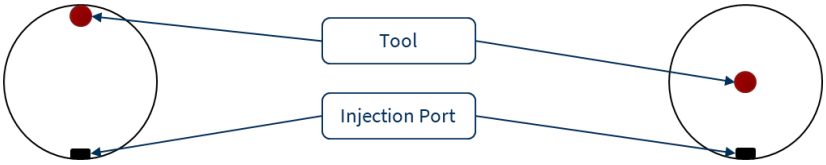

(a) **(b)**

Figure 10: tool position during the dynamic measurement as seen from the cross section: (a) opposite the injection port, and (b) centralized.

The results of the dynamic measurements taken at both positions are shown in Figure 11. The measured voltage from the tool was converted into chloride concentration using Equation 1. Both measurements successfully captured the drop in voltage around the injection port, indicating a spike of chloride concentration around that depth. The calculated chloride concentration also showed promising results, being close to 0 mol/L below the feed zone, but higher values around and above the feed zone shows. However, a portion of the calculated chloride concentration around and above the feed zones were found to be higher than the possible value of 0.05 mol/L, which is the chloride concentration that was being injected.

Additionally, it was also observed that the centralized position generally measures higher concentration at similar depths compared to the first position, which indicated that less mixing happened further away from the feed zone. Furthermore, it was noticed that there was a delay in the response of the tool shown by the consistently different depth of calculated chloride concentration peak between the RIH and POOH. The RIH measurement suggested a peak below the feed zone, while the POOH shows it above the feed zone. These findings indicate that dynamic measurement protocols need to be incorporated, especially regarding the time response and chloride concentration accuracy.

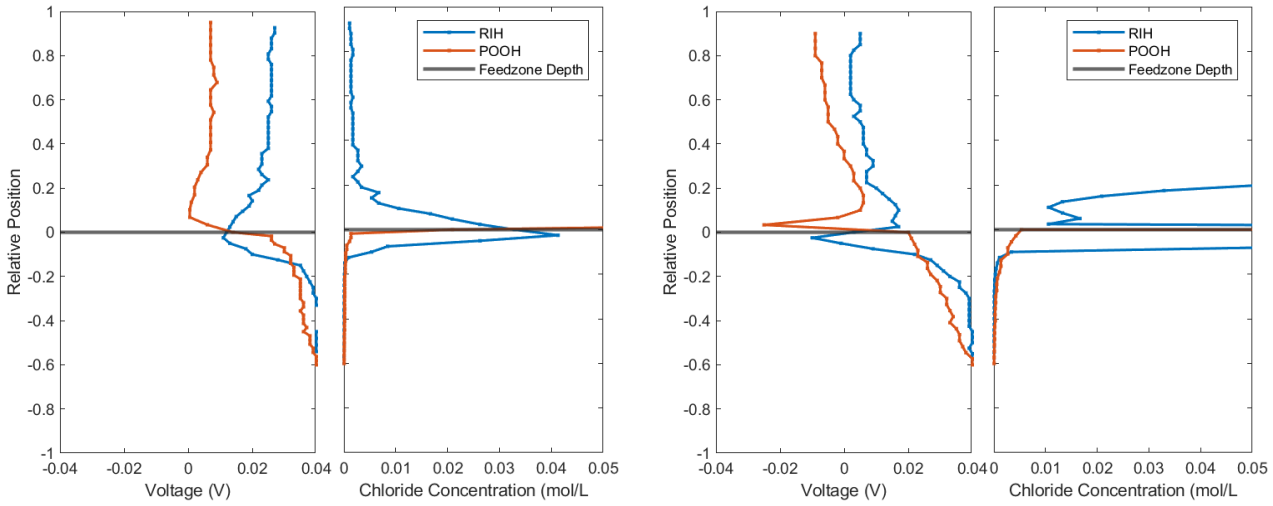

Figure 11: Dynamic measurement result (a) at the opposite wall from the feed zone inlet, and (b) at the center of the wellbore.

4. NUMERICAL FLOW SIMULATION UPDATE

The updated study aimed to overcome the discrepancy between numerical simulations and laboratory experiments while also expanding the approach to now consider the disturbed state, i.e., the state where the flow behavior in the wellbore is affected by the presence of the chloride tool. To better reflect the artificial well system in the laboratory, modifications to the geometry setup for the numerical simulations were conducted. As shown in Figure 12, the feed zone radius is now slightly smaller at 0.5 cm and the well radius is larger at 7.5 cm.

Table 2 describes the three new case groups that were added. Case group S1-L5 examined a smaller feed zone radius at 0.7 cm, 0.5 cm, and 0.1 cm, where the S1-L15-0 case with 0.7 cm radius is the control case of the previous geometry setup. The simulation run on an increasingly smaller feed zone radius was conducted to understand the smallest resolution at which the chloride tool could detect a feed zone. Meanwhile, the S1-L6 case group replayed the S1-L4 cases with a new wellbore radius at 7.5 cm, a new feed zone inlet radius at 0.5 cm, and a denser feed zone inflow rate range between 20 ml/s to 200 ml/s. Finally, the S1-L7 case group simulated the disturbed state, which is the state where the chloride tool is placed near the feed zone inlet and thus disturbed the flow inside the wellbore. The schematic for the disturbed state cases is shown in Figure 13.

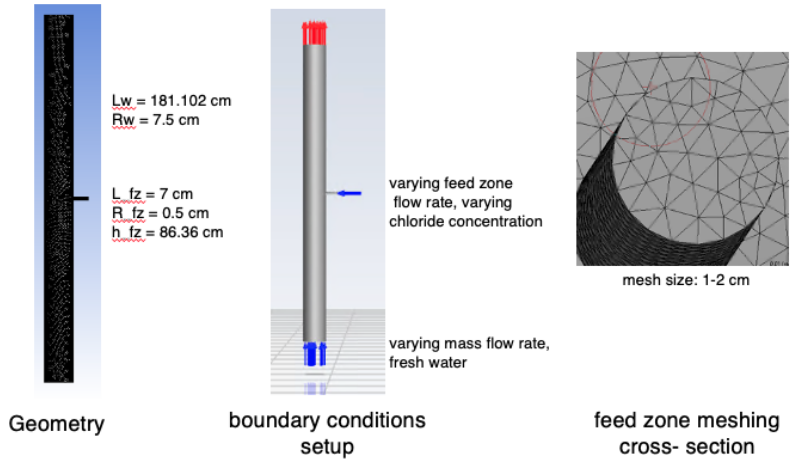

Figure 12: Updated geometry setup and boundary conditions of Model S1 at laboratory scale

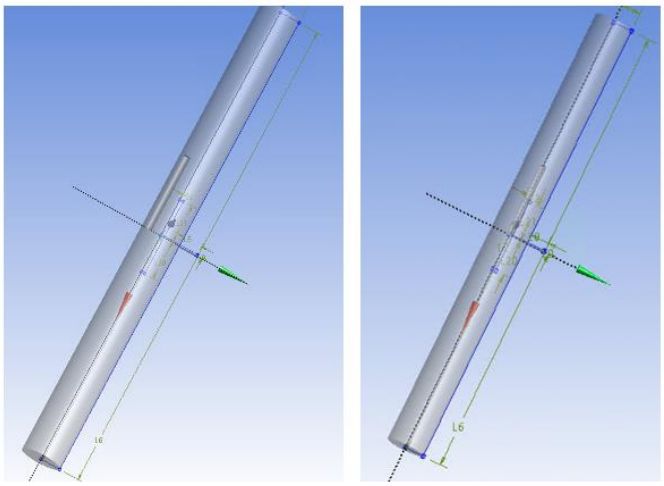

Figure 13: Schematics and description for the disturbed state case group S1-L7

Table 2: Additional Simulation Case Parameters

Case ID	S1-L5-]0 to 2]	S1-L6-[1 to 9]	S1-L7-[1 to 2]
Scale	Lab scale	Lab scale	Lab scale
Description	Testing different feed zone radius: 0 - R = 0.7 cm 1 - R = 0.5 cm 2 - R = 0.1 cm	Updated geometry setup with different inlet velocity	Disturbed state with stationary chloride tool. Tool position is in the center for case 2a and 2b and 5 cm from the wall at the opposite of the inlet (wall-line-4) for case 1a and 1b.
Wellhead	Open	Open	Open
Main wellbore mass rate	2.09 kg/s	2.09 kg/s	1a & 2a - 2.09 kg/s 1b & 2b – 0 kg/s (no internal flow)
Feed zone flow rate	112.2 ml/s (mimicking lab experiments)	1 - 112.2 ml/s 2 - 125 ml/s 3 - 150 ml/s 4 - 175 ml/s 5 - 200 ml/s 6 - 20 ml/s 7 - 50 ml/s 8 - 75 ml/s 9 - 100 ml/s	112.2 ml/s (mimicking lab experiments)
Δm (kg/s)	1.98	1 – 1.98 2 – 1.96 3 – 1.94 4 – 1.91 5 – 1.89 6 – 2.07 7 – 2.04 8 – 2.01 9 – 1.99	1a & 2a– 1.98 1b & 2b – (-0.112)
NaCl concentration at feedzone	0.05 mol/L	0.05 mol/L	0.05 mol/L
NaCl concentration delta (mol/L)	0.05	0.05	0.05

The simulation results of different feed zone inlet radius shown in Figure 14 revealed that a slight decrease of radius from 0.7 cm (S1-L5-0) to 0.5 cm (S1-L5-1) resulted in a stronger inlet flow that can reach the opposite wall. However, too small of a radius will prevent the inlet fluid from entering the main wellbore as the feed zone flow is weaker than the wellbore's internal flow, as shown in case S1-L5-3.

It should be noted that S1 cases were set up with point-source feed zones; other possible feed zone geometries like inclining planes that resemble a fracture intersection may behave differently from the S1-L5 case groups.

Updated well system geometry resulted in a new base case S1-L6-1 which better describes the laboratory experiments. Features previously only seen in the S1-L4-4 with a 200 ml/s inflow rate, such as the prominent blind spot and downward distribution, can now be seen at a lower inflow rate of 112.2 ml/s. Furthermore, a comparison of laboratory experiment cross sectional view footage from section 3.2 with the horizontal sections of the feed zone fluid volume fraction in S1-L6-1 case (Figure 15) shows consistent behavior of blind spot formation and inflow fluid reaching the opposite wall followed by circling the perimeter. These similarities mark a step forward in bringing the laboratory experiment and numerical simulation aligned.

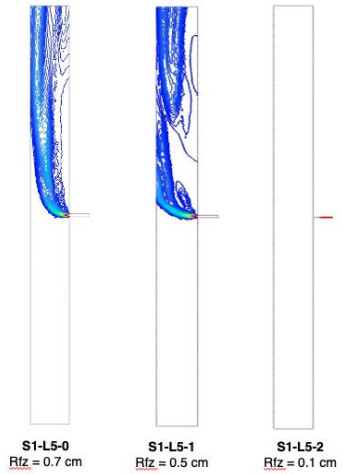

Figure 14: Laboratory experiment recorded from the top of the well compared with XY sections of the undisturbed state base case S1-L16-1 at different z-offsets. The contours show the volume fraction of the inflow fluid, which is a NaCl solution of 0.05 mol/L concentration.

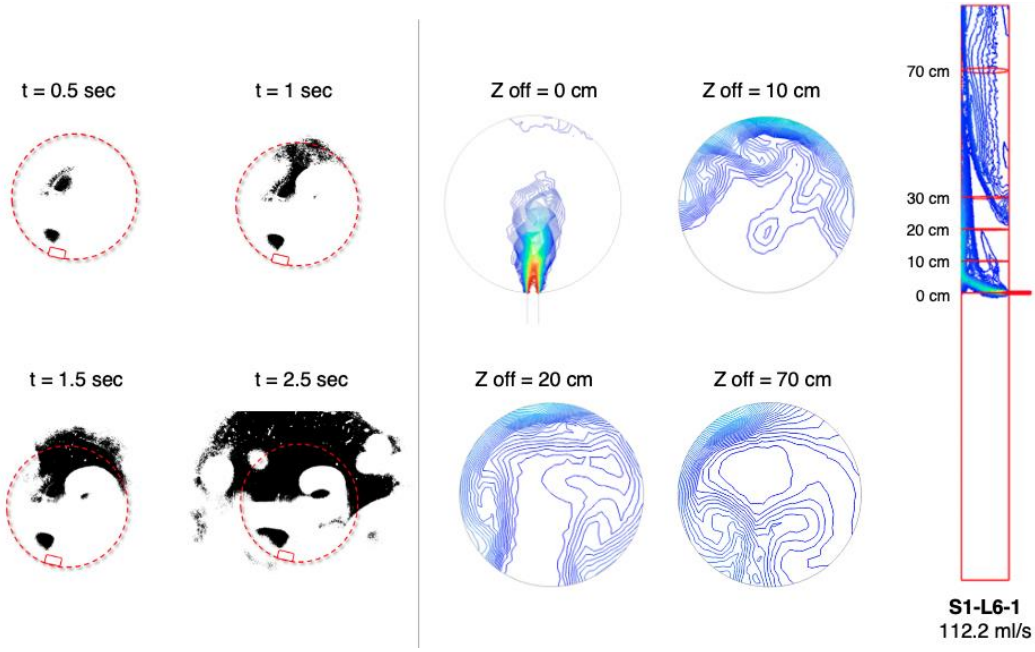

Figure 15: Laboratory experiment results recorded from the top of the well compared with horizontal sections of the undisturbed state base case S1-L16-1 at different z-offsets. The contours show the volume fraction of the inflow fluid, which is a NaCl solution of 0.05 mol/L concentration.

Simulated chloride concentration distribution of different inflow rates across S1-L6 case groups are summarized in Figure 16. The results are extracted from the wall-line-4 position, which is the position across from the feed zone inlet. The inflow rates are grouped into the high-flowrate group for those more than 112.2 ml/s and the low-flowrate group for those less than 112.2. ml/s. While the high-flowrate group exhibits a clear pattern across the z-direction, i.e., spike of chloride concentration in front of the feed zone followed by a decrease

zone and a rebound zone, the low-flowrate group's pattern is less apparent and more inconsistent. One feature common in both high-flowrate and low-flowrate groups is the inlet front chloride peak, which is promising as we can expect that the chloride tool can consistently locate the feed zone inflow. A similar inlet peak pattern marking the position of the feed zone was also observed in the dynamic measurement experiment detailed in Section 3.3 and shown in Figure 11a where the tool was also positioned similarly to the wall-line-4 position.

In addition, it was also observed that the simulated chloride concentration at the wall-line-4 position under various flow rates displays concentration range between 0.01 to 0.017 mol/L, which was 20% to 34% of the actual injected chloride concentration of 0.05 mol/L. While it is understood that the dispersed feed zone inflow will inevitably result in diluted chloride concentration when measured at any location of the wellbore except right in front of the inlet, it is expected that the discrepancy will be less pronounced and more consistent in the disturbed state simulation, especially when the tool is positioned at the center of the wellbore. In actual deployment, there will need to be a compensating correction to the estimated chloride concentration values.

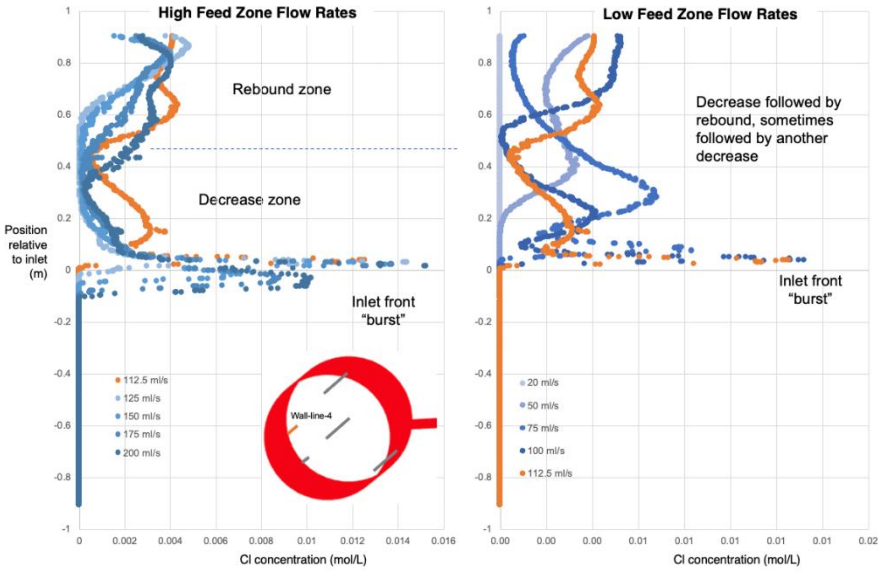

Figure 16: Comparison of the undisturbed state case S1-L6-1 and the Cl concentration change along the wellbore height at different feed zone flow rates. The results are extracted from the wall-line-4 position across the feed zone inlet. The left image shows the base case inlet flow rate (112.2 ml/s) and higher, while the right image shows the base case flow rate and lower.

Further comparison was conducted for the S1-L6 case groups by examining the impact of different tool positions on the cross-sectional area of the wellbore, as shown in Figure 17. It was found that extracting the chloride concentration results from positions within the feed zone jet, such as from the center of the wellbore (midline position) and the opposite wall (wall-line-4), will produce the inlet front peak pattern that is valuable in locating and quantifying the feed zone inflow. In contrast, the results extracted from outside the jet will hide the inlet front peak pattern, making it challenging to locate the feed zone and measure the flow rate. Thus, the tool design must be able to ideally place the tool firmly within the jets of feed zones along the well, which can be positioned anywhere at the circumference of the wellbore. This can be accomplished by keeping the tool at the center of the wellbore using a centralizer.

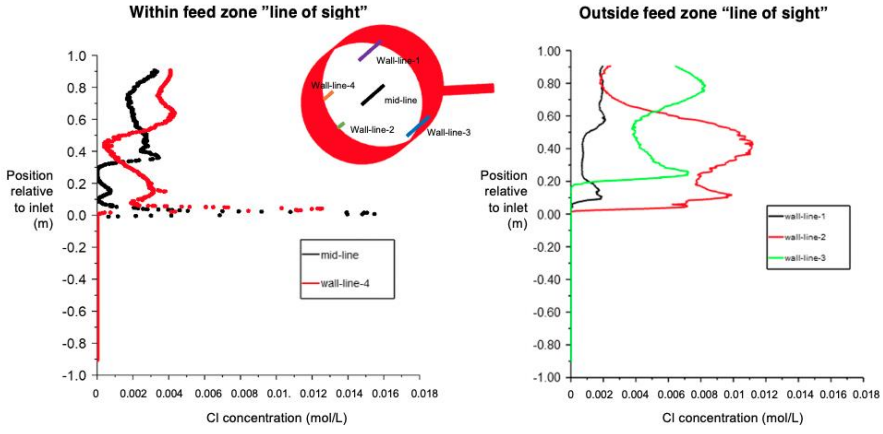

Figure 17: Comparison of the undisturbed state case S1-L6-1 and the Cl concentration change along the wellbore height.

The simulation results of the disturbed state case groups S1-L7 taken from the horizontal section are shown in Figure 18, while the same results in the horizontal section intersected right at the feed zone height are shown in Figure 19. Note that the disturbed state is the most comparable simulation to the dynamic measurement experiment. It can be observed that having the tool placed near the feed zone will pose a significant disturbance to the flow behavior within the wellbore in a positive manner. For instance, putting the tool at the wellbore center (S1-L7-2a) makes the chloride concentration more prominent and closer to the actual inflow concentration at 70-100%. Similarly, placing the tool in the opposite wall (S1-L7-1a) also increases the inflow concentration significantly up to 50%. This finding further supports the use case for a centralizer in the tool design.

Moreover, the S1-L7-1a case can also be compared to the dynamic measurement experiment with similar positioning outlined in Section 3.3, although the peak concentration registered during the experiment is much higher than the simulation. Although the inclination is to mark the simulation as underestimating chloride concentration, it is also possible that the calibration equation (Equation 1) needs to be adjusted, as it yields a higher than maximum possible value for when the tool is centered during the dynamic measurement thus overestimating the experiment readings. For the same reason, S1-L7-2a can only be compared qualitatively.

The results of similar tool placements but with no internal wellbore flow (S1-L7-1b and S1-L7-2b) are also displayed (Figure 18). With the lack of upflow, the feed zone fluid is dispersed in all directions instead of uniformly, resulting in a concentration between 30-70%, with inlet flow peak still observed at around 70% concentration. Thus, variation in the internal wellbore flow will affect the quantification of the chloride concentration and, subsequently, the flow rate estimation.

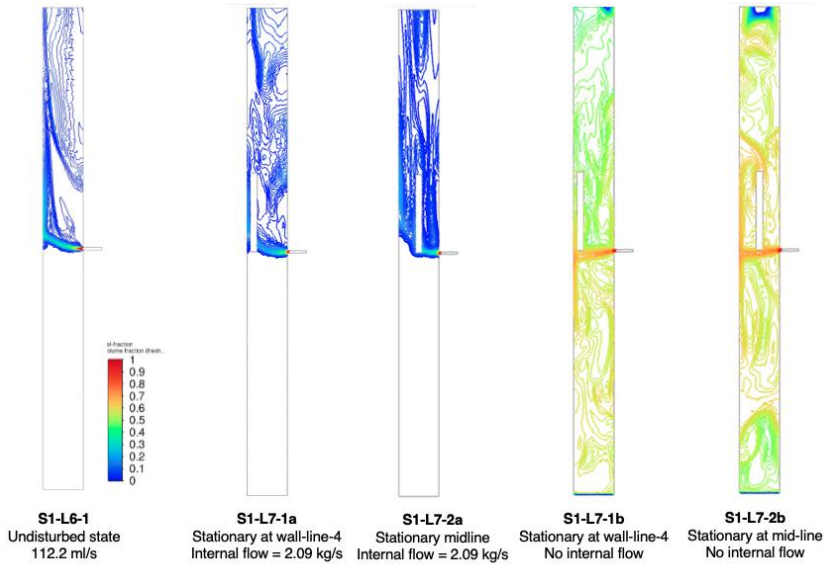

Figure 18: Comparison of the disturbed state case group (S1-L7), XZ section. The contours show the volume fraction of the inflow fluid, which is a NaCl solution of 0.05 mol/L concentration.

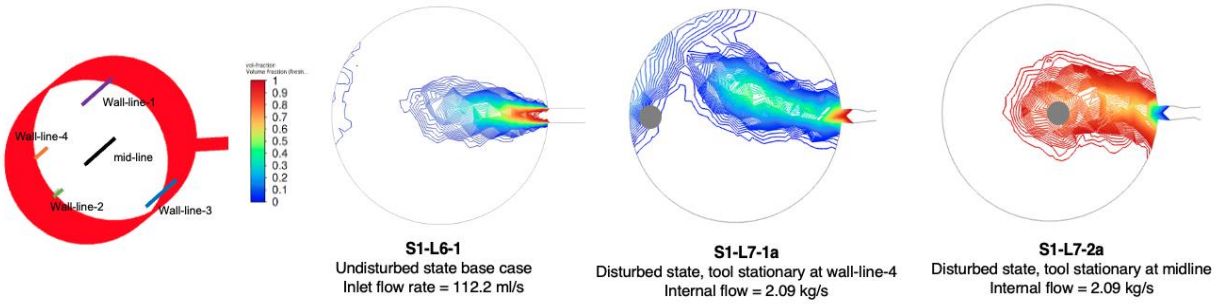

Figure 19: The XY section of the disturbed state cases S1-L7-1a and S1-L7-2a compared with the undisturbed state base case S1-L6-1. Reference to tool position naming is shown in the top left. The contours show the volume fraction of the inflow fluid, which is a NaCl solution of 0.05 mol/L concentration.

In summary, incorporating the disturbed state in the simulation provides a more realistic simulation and allows for better comparison to actual experiments. Future simulations will be improved further by including the wireline assembly design with additional housing units and mixers.

5. CONCLUSION

An updated version of the chloride tool is being developed and will be tested under high-pressure and high-temperature conditions to evaluate its performance. The tool will be specifically tested at 207 MPa and 225°C. This new version of the tool is being built upon recent progress outlined in research papers by Sausan et al. (2022) and Judawisastra et al. (2022). In order to understand the flow behaviors of the tool, a closer examination of the dye-tracer experiment in a horizontal cross section has been performed. This experiment was conducted in a laboratory setting and dynamic measurements were taken with the tool positioned at the wellbore center and at the wall opposite to the feed zone inlet. Additionally, comparable cases were also simulated numerically for verification. The overall simulation results of the disturbed state (i.e., the state when the tool is in place) agreed with the dynamic measurement in the laboratory, especially on having the peak chloride concentration measured at the feed zone height. However, small differences were found in the measured concentration, which suggests that the calibration equation should be adjusted, especially considering the overestimation that was registered when the tool was placed at the center. Simulations also showed that measurement zones apparent in the high inlet flowrate cases are less prominent in the low inlet flowrate cases, although the inlet front peak can still be detected. Furthermore, simulation of various tool position scenarios indicated inlet front peaks only being seen within the feed zone region. Overall, the recent findings support the inclusion of a centralizer for the wireline tool design to increase the consistency and precision of the chloride concentration calculation. This will help ensure that the tool is able to provide accurate and reliable measurements under high-pressure and high-temperature conditions.

ACKNOWLEDGEMENT

This work is part of the Utah FORGE project under award number 3-2418 as a collaborative project between Stanford University and Sandia National Laboratory, supported by the U.S. Department of Energy. Sandia National Laboratories is a multimission laboratory managed and operated by National Technology & Engineering Solutions of Sandia, LLC, a wholly owned subsidiary of Honeywell International Inc., for the U.S. Department of Energy's National Nuclear Security Administration under contract DE-NA0003525. This paper describes objective technical results and analysis. Any subjective views or opinions that might be expressed in the paper do not necessarily represent the views of the U.S. Department of Energy or the United States Government. (SAND2023-11368C)

REFERENCES

Acuña, J. A. and. Arcedera B. A,: Two-Phase Flow Behavior and Spinner Data Analysis In Geothermal Wells, Proceedings 13th Workshop on Geothermal Reservoir Engineering, Stanford University, Stanford, California (2005).

Cieslewski, G., Hess, R. F., Boyle, T. J., Yelton, W. G.: Development of a Wireline Tool Containing an Electrochemical Sensor for Real-time pH and Tracer Concentration Measurement, GRC Transactions, Vol.40, (2016).

Corbin, W. C., Cieslewski G., Hess R. F., Klamm B. E., Goldfarb L., Boyle T. J., and Yelton W.G.: Development of a Downhole Tool for Measuring Enthalpy in Geothermal Reservoirs, 42nd Workshop on Geothermal Reservoir Engineering, Stanford University, Stanford, CA (2017).

Gao, X., Egan, S., Corbin, W.C., Hess, R.F., Cieslewski, G., Cashion, A.T., and Horne, R.N.: Analytical and Experimental Study of Measuring Enthalpy in Geothermal Reservoirs with a Downhole Tool, GRC Transactions, Vol.41, (2017).

Huenges, E.: 25 - Enhanced geothermal systems: Review and status of research and development, Geothermal Power Generation, Woodhead Publishing, Pages 743-761, (2016).

Judawisastra, L. H., Sausan, S., Horne, R. N.: Analytical, Experimental and Numerical Development Update on Inflow Measurement in Geothermal Wells from Chloride Concentration. Proceedings, 8th Indonesia International Geothermal Convention & Exhibition, (2022).

Sausan, S., Judawisastra, L. H., Horne, R. N.: Development of Downhole Measurement to Detect Inflow in Fractured Enhanced Geothermal Systems (EGS) Wells, Proceedings 47th Workshop on Geothermal Reservoir Engineering, Stanford University, Stanford, California (2022).